

3-D PTV measurement of Marangoni convection in liquid bridge in space experiment

Taishi Yano · Koichi Nishino · Hiroshi Kawamura ·
Ichiro Ueno · Satoshi Matsumoto · Mitsuru Ohnishi ·
Masato Sakurai

Received: 31 December 2010 / Revised: 17 April 2011 / Accepted: 30 May 2011 / Published online: 30 June 2011
© Springer-Verlag 2011

Abstract Microgravity experiments have been conducted on the International Space Station in order to clarify the transition processes of the Marangoni convection in liquid bridges of high Prandtl number fluid. The use of microgravity allows us to generate large liquid bridges, 30 mm in diameter and up to 60 mm in length. Three-dimensional particle tracking velocimetry (3-D PTV) is used to reveal complex flow patterns that appear after the transition of the flow field to oscillatory states. It is found that a standing-wave oscillation having an azimuthal mode number equal to one appears in the long liquid bridges. For the liquid bridge 45 mm in length, the oscillation of the flow field is observed in a meridional plane of the liquid bridge, and the flow field exhibits the presence of multiple vortical structures traveling from the heated disk toward the cooled disk. Such flow behaviors are shown to be associated with the propagation of surface temperature fluctuations visualized with an IR camera. These results indicate that the

oscillation of the flow and temperature field is due to the propagation of the hydrothermal waves. Their characteristics are discussed in comparison with some previous results with long liquid bridges. It is shown that the axial wavelength of the hydrothermal wave observed presently is comparable to the length of the liquid bridge and that this result disagrees with the previous linear stability analysis for an infinitely long liquid bridge.

List of symbols

Ar	Aspect ratio [–]
D	Disk diameter [m]
f	Frequency [Hz]
H	Length of the liquid bridge [m]
m	Azimuthal mode number [–]
Ma	Marangoni number [–]
Ma_c	Critical Marangoni number [–]
Pr	Prandtl number [–]
r	Radial position [m]
t	Time [s]
T	Oscillation period [s] or temperature [K]
T_c, T_h	Cooled-disk temperature and heated-disk temperature [K]
ΔT	Temperature difference [K]
ΔT_c	Critical temperature difference [K]
V	Liquid bridge volume [m ³]
V_0	Gap volume [m ³]
V_r	Volume ratio ($=V/V_0$) [–]
z	Axial position [m]

Greek symbols

α	Thermal diffusivity [m ² /s]
λ_z	Axial wavelength [m]
ν	Kinematic viscosity [m ² /s]
ρ	Density [kg/m ³]

T. Yano · K. Nishino (✉)
Department of Mechanical Engineering,
Yokohama National University, 79-5 Tokiwadai, Hodogaya-ku,
Yokohama, Kanagawa 240-8501, Japan
e-mail: nish@ynu.ac.jp

H. Kawamura
Department of Mechanics and System Design,
Tokyo University of Science, Suwa, 5000-1 Toyohira, Chino,
Nagano 391-8502, Japan

I. Ueno
Department of Mechanical Engineering,
Tokyo University of Science, 2641 Yamazaki, Noda,
Chiba 278-8510, Japan

S. Matsumoto · M. Ohnishi · M. Sakurai
Japan Aerospace Exploration Agency, 2-1-1 Sengen,
Tsukuba, Ibaraki 305-8505, Japan

- σ Surface tension [N/m]
 σ_T Temperature coefficient of surface tension [N/(m·K)]

Superscripts

- ($\bar{\quad}$) Mean value
 (\sim) Dimensionless value

1 Introduction

Marangoni convection is the flow driven by the surface-tension gradient along a liquid-free surface. Marangoni convection becomes of importance in liquid films, droplets, bubbles, and liquid bridges where the surface-tension gradient is caused by the temperature and concentration gradients along liquid-free surfaces. The liquid bridge is the geometry that is seen in the floating-zone method for crystal growth. In this method, the feed material for crystal growth is heated by a ring heater, and the melt in the form of liquid bridge is suspended between the feed rod and the grown crystal. The liquid bridge is subjected to a steep temperature gradient along the liquid-free surface. This flow configuration is modeled to a liquid bridge suspended between two concentric disks heated differentially. This simplified flow configuration is called a half-zone liquid bridge, and the temperature difference between the disks, ΔT , is the driving force for the Marangoni convection.

As reviewed by Ostrach (1983), Kuhlmann (1999), and Kawamura and Ueno (2006), a large number of studies have been conducted in order to clarify the characteristics of Marangoni convection in the half-zone liquid bridge. Particular attention has been paid to the instability mechanisms and to the resultant features of temperature and flow fields in the liquid bridge. The instability appears as a transition from a steady, axisymmetric flow field to an oscillatory, nonaxisymmetric one. Such a transition takes place when ΔT exceeds a critical value, ΔT_c . The conditions for the onset of transition are dependent on the fluid properties, the length and the shape of the liquid bridge, the surrounding gas motion, and so on. The clarification of the onset conditions has been the central issue in the study of Marangoni convection in the half-zone liquid bridge. For example, latest results obtained from ground experiments can be found in Shevtsova et al. (2011).

Two series of microgravity experiments have been conducted as the first science experiment on the Japanese Experimental Module “KIBO” of the International Space Station (ISS). The overview of these microgravity experiments was reported by Kawamura et al. (2010). The purpose of this space experiment is to accumulate data on the following phenomena in long liquid bridges (up to 60 mm in length) that can be formed only in a long-period microgravity environment in ISS:

1. the onset of oscillatory Marangoni convection,
2. the transition to chaotic and turbulent states, and
3. the formation of particle accumulation structures.

The present paper is to report the characteristics of oscillatory flow fields measured by using three-dimensional particle tracking velocimetry (3-D PTV). This technique, developed originally by Nishino et al. (1989), is customized for the space experiment, so that a fully automated image acquisition for camera calibration and particle tracking can be done without suffering from vibration of the liquid bridge. To do so, the flow field is observed through a transparent disk that is used for the formation of the liquid bridge, as demonstrated by Nishino et al. (1995) in their short-period microgravity experiment during parabolic flight of an aircraft. This approach was shown by Nishimura et al. (2005) to be useful for the measurement of small liquid bridges that are formed in their ground experiments. The oscillatory flow fields revealed in the present study are discussed in conjunction with surface temperature fluctuations visualized with an infrared (IR) camera. The comparison is made with the results reported by Xu and Davis (1984) and Schwabe (2005), where the former performed a linear stability analysis of an infinity long liquid bridge of high Pr fluids with an imposed axial temperature gradient while the latter conducted a sounding rocket experiment with a long liquid bridge of 2cSt silicone oil ($Pr = 28.0$). The present results have shown the axial propagation of hydrothermal wave (HTW hereafter) in the direction toward the cooled disk. The HTW is found to be associated with vortical structures in the liquid bridge and also with an inclined wavefront of surface temperature fluctuations. The features of velocity and temperature fields are discussed in some detail.

2 Methods

2.1 Liquid bridge and experimental conditions

A liquid bridge of silicone oil is formed between two coaxial disks heated differentially. The geometry of the liquid bridge is illustrated in Fig. 1. The heated disk is made of transparent sapphire so that the CCD cameras can view the flow field through the disk. The cooled disk is made of aluminum. Both disks are 30 mm in diameter, and they have a 45° edge to prevent liquid leakage. The cooled disk is traversable in the axial direction, and a wide range of aspect ratio, $Ar (=H/D)$, can be realized, where H and D are the length of the liquid bridge and the diameter of the disk, respectively. The maximum Ar in the present study is 2.0. The volume ratio, $Vr (=V/V_0)$, is 0.95, where V and V_0 are the volume of the liquid and that of the gap between the

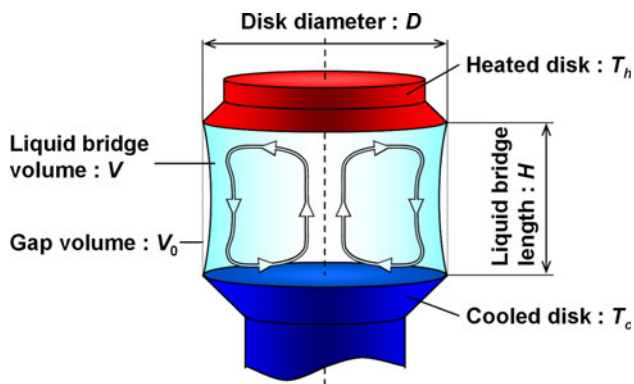


Fig. 1 Geometry of the liquid bridge in the half-zone method

disks ($V_0 = D^2H/4$). The condition for $Vr = 1.00$ gives a straight cylindrical shape, and the present value, which is slightly lower than 1.00, is chosen to avoid possible fluid leakage through the edge of the disks.

Silicone oil of 5cSt ($=5 \times 10^{-6} \text{m}^2/\text{s}$) in kinematic viscosity at 25°C (Shin-Etsu Chemical Co., Ltd, KF-96L) is used as working fluid. Its Prandtl number, Pr , is 67.0 at 25°C. The surface tension, σ , and its temperature coefficient, σ_T , are $19.7 \times 10^{-3} \text{N/m}$ and $-6.23 \times 10^{-5} \text{N}/(\text{m K})$, respectively. The fluid is transparent and therefore suitable for flow visualization. Approximately 500 tracer particles are introduced in the fluid. Their average diameter and density are 180–200 μm and 1,300 kg/m^3 , respectively. Rather, large particles are selected to facilitate visualization of particle motions for 3-D PTV. Each particle is coated with gold-nickel alloy, and the density ratio of the particle to the silicone oil is about 1.4.

The critical temperature difference, ΔT_c , for the onset of oscillatory flow and temperature fields in the liquid bridge is determined by giving a stepwise increase in the temperature difference, ΔT , between the disks (i.e., $\Delta T = T_h - T_c$). This is achieved by keeping T_c constant at 20°C and by increasing T_h in a stepwise manner. The average of T_h and T_c is, therefore, $\bar{T} = (T_c + T_h)/2 = 20^\circ\text{C} + \Delta T/2$. A sufficiently long waiting time (more than 30 min) is given after each stepwise increase in ΔT . The onset of oscillation is detected from several observations such as the temperature signal from a fine thermocouple sensor placed in the liquid, the particle motions taken by the cameras for 3-D PTV, and the dye traces visualized in the photochromic dye activation technique. All these observations provided consistent detection of the onset condition in the present experiments. The determined values of ΔT_c are plotted as a function of Ar in Fig. 2. The experimental conditions for the second series of the present space experiment are mentioned in this section. The experimental conditions for the first series are the same as those for the second ones except for a slight difference in σ_T , which is -6.58×10^{-5}

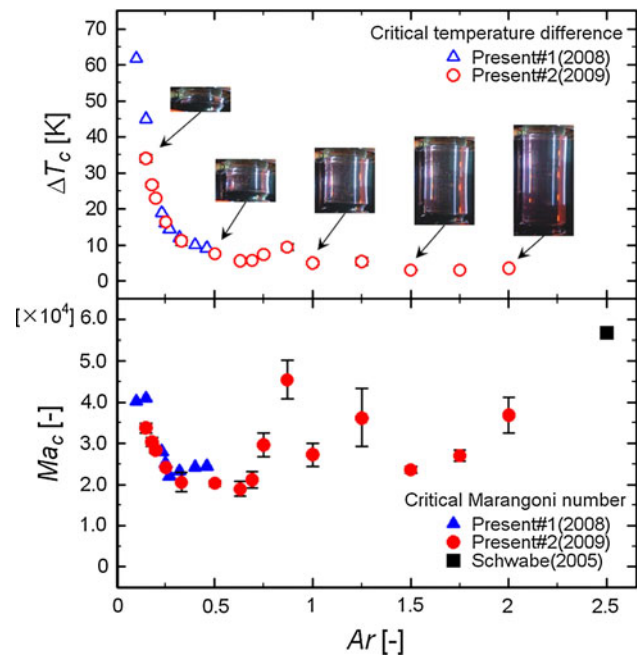


Fig. 2 Plot of ΔT_c and Ma_c as a function of Ar

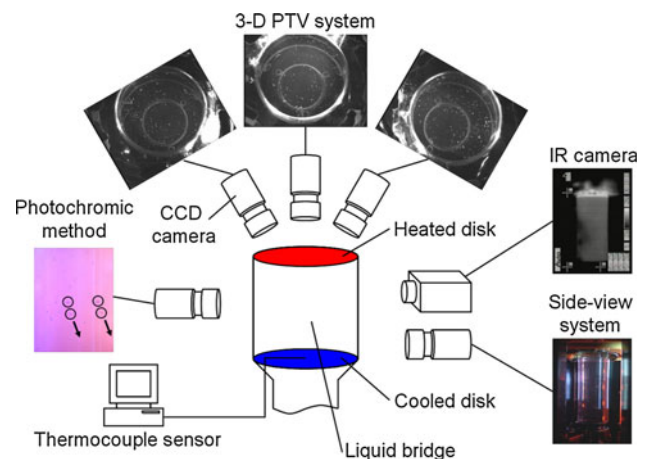


Fig. 3 Schematic diagram of the measurement apparatuses installed in FPEF

$\text{N}/(\text{m K})$. The Marangoni number, Ma , is defined from ΔT as follows:

$$Ma = \frac{|\sigma_T| \Delta T H}{\rho \bar{\nu} \alpha} \tag{1}$$

where ρ , α , and $\bar{\nu}$ are the density, the thermal diffusivity, and the mean kinematic viscosity of the fluid, respectively. In the present experiments, $\rho = 915 \text{kg}/\text{m}^3$ and $\alpha = 7.5 \times 10^{-8} \text{m}^2/\text{s}$, while the value of $\bar{\nu}$ is the mean of $\nu(T_h)$ and $\nu(T_c)$ and therefore dependent on the disk temperatures. In Fig. 2, the measured Ma_c is plotted as a function of Ar . Also included is the result measured by Schwabe (2005) in his sounding rocket experiment with a liquid bridge of 2cSt

silicone oil and $Ar = 2.5$. Note that the conditions for large Ar (say, $Ar > 1.50$) were examined previously only in microgravity environment.

2.2 3-D PTV for space experiment

3-D PTV is a simple and effective technique for measuring flow patterns in 3-D complex flows. More than two cameras, often three cameras, are used for image acquisition of tracer particles suspended in the fluid (e.g., Nishino et al. 1989; Mass et al. 1993). Once the images of tracer particles together with those for camera calibration are acquired, 3-D trajectories of tracer particles are determined and 3-D flow patterns are revealed. Such simplicity provides a definite advantage of 3-D PTV as a tool for the space experiment where the fully automated operation of the experimental apparatuses is necessary.

The original hardware design of 3-D PTV was studied by Nishino et al. (1995). They carried out microgravity experiments in parabolic flight of an aircraft in order to generate large liquid bridges of 15cSt silicone oil between a transparent glass disk and an opaque copper disk. Their diameter was 30 mm. Three finger-sized B/W CCD cameras were mounted near the glass disk so that the flow field in the liquid bridge was visible even in the period when the liquid bridge was significantly deformed by the variation of

g-level in the aircraft. This hardware design was adopted in the sounding rocket experiment done by Nishino et al. (1998), where a liquid bridge of 2cSt silicone oil was suspended between 28 mm-diameter disks.

Basically, the same hardware design was used for 3-D PTV for the present space experiment. Three finger-sized B/W CCD cameras (768×494 pixels and 30fps) are mounted in Fluid Physics Experiment Facility (FPEF). The cameras can observe the flow field in the liquid bridge through a transparent sapphire disk 30 mm in diameter. The illumination is given by a Xenon strobe lamp, and the flash light is given from the side of the liquid bridge by using flexible fiber light guides. Figure 3 is the schematic diagram of the measurement apparatuses installed in FPEF. An IR camera having a wavelength sensitivity of 8–14 μm is installed to visualize the surface temperature of the liquid bridge. As depicted in the figure, an apparatus for the photochromic dye activation technique is also installed for the visualization of surface velocity of the liquid bridge. As shown later, this technique was found to provide the most sensitive method for the detection of the onset of oscillation. All the images acquired at 30fps during experiment are stored in the hard drive recording system, and they are transferred from ISS to the ground for data analysis. The data analysis for 3-D PTV consists of four procedures as follows: (1) preprocessing of particle images, (2) camera calibration, (3) particle tracking, and (4) 3-D reconstruction.

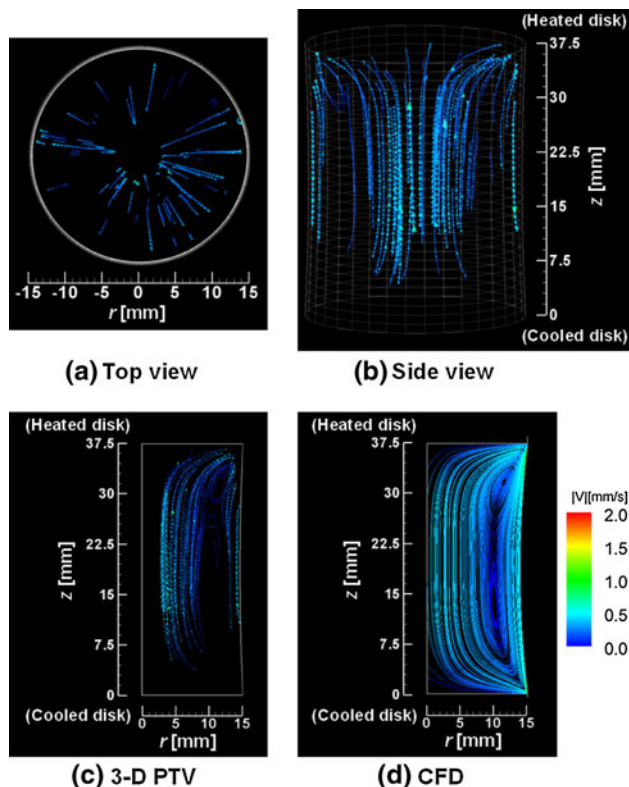


Fig. 4 Particle trajectories for $Ar = 1.25$ and $\Delta T = 2.9$ K; (a–c) those measured by using 3-D PTV, (d) those predicted with CFD

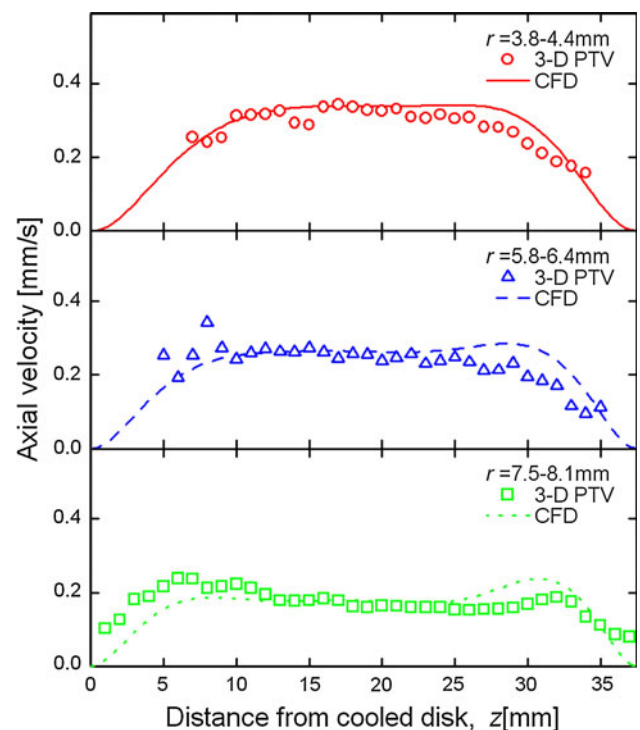


Fig. 5 Axial velocity as a function of the distance from the cooled disk

Their details are reported by Yano et al. (2010a, b), and therefore, they are not repeated here.

2.3 CFD method for comparison

For verification purpose, the results of 3-D PTV are compared with the numerical results that are obtained by using a commercial CFD software (STAR-CCM+). Only a laminar state at $Ar = 1.25$ and $\Delta T = 2.9$ K ($Ma = 1.90 \times 10^4$) is considered, and the symmetry of flow and temperature field about the axis of the liquid bridge is assumed. The surface shape of the liquid bridge for $Vr = 0.95$ is determined by solving the Young–Laplace equation. The computational grids are defined both in the liquid and in the surrounding gas. The total number of grids is 15040 in the plane of symmetry. Since the software is incapable of handling the thermocapillary boundary condition at the liquid–gas interface, the surface-tension difference is given as a body force exerting in a layer of very thin grids adjacent to the liquid–gas interface. The finite volume method is used for the solution of the governing equations, i.e., the continuity equation, the momentum equation for incompressible flow, and the energy equation, for both domains of liquid and gas. More details of the CFD methods can be found in Tiwari and Nishino (2007), who used an early and simplified version of STAR-CCM+.

3 Result and discussion

3.1 Steady flow and verification

Figure 4 shows the present result for $Ar = 1.25$ and $\Delta T = 2.9$ K ($Ma = 1.90 \times 10^4$). This temperature difference is smaller than the critical value ($\Delta T_c = 5.4$ K).

Therefore, the flow pattern is steady, and the presence of an axisymmetric 2-D velocity field is evident. Figure 4c, d shows the particle trajectories for comparison between the present result and the CFD result mentioned above. The particle trajectories look very similar to each other, and they reveal the presence of two vortices, one near the heated disk and the other in the lower part of the liquid bridge. The appearance of two vortices was reported by Chernatinsky et al. (2002) in their CFD result. Such a flow pattern is called multi-roll structure, and it is considered to be unique for high Ar liquid bridges (Schwabe 2005). For verification of the present measurement, the measured profiles of axial velocity are compared with the CFD results. The comparison is shown in Fig. 5, where the velocity profiles at several radial positions (i.e., $r = 3.8$ – 4.4 mm, 5.8 – 6.4 mm, and 7.5 – 8.1 mm) are plotted as a function of the distance from the cooled disk. Reasonable agreement is recognized, particularly in the profiles near the middle height of the liquid bridge. The standard deviation of the difference between the measurement and the CFD is less than 0.043 mm/s, which is less than 20% of the maximum velocity shown here. Note that the two peaks in the profile for $r = 7.5$ – 8.1 mm, one at $z = 7.5$ mm and the other at $z = 32.5$ mm, should be related to the local maxima of surface velocity, which are known to exist for high Pr liquid bridges (e.g., Tiwari and Nishino 2007). These results confirm the overall validity of the present 3-D PTV measurement.

3.2 Oscillatory flow

3.2.1 $Ar = 0.75$

Figure 6 shows the particle trajectories measured just after the transition to oscillatory state occurs, where $Ar = 0.75$ and $\Delta T = 7.9$ K ($Ma = 3.25 \times 10^4$, $Ma/Ma_c = 1.09$). The

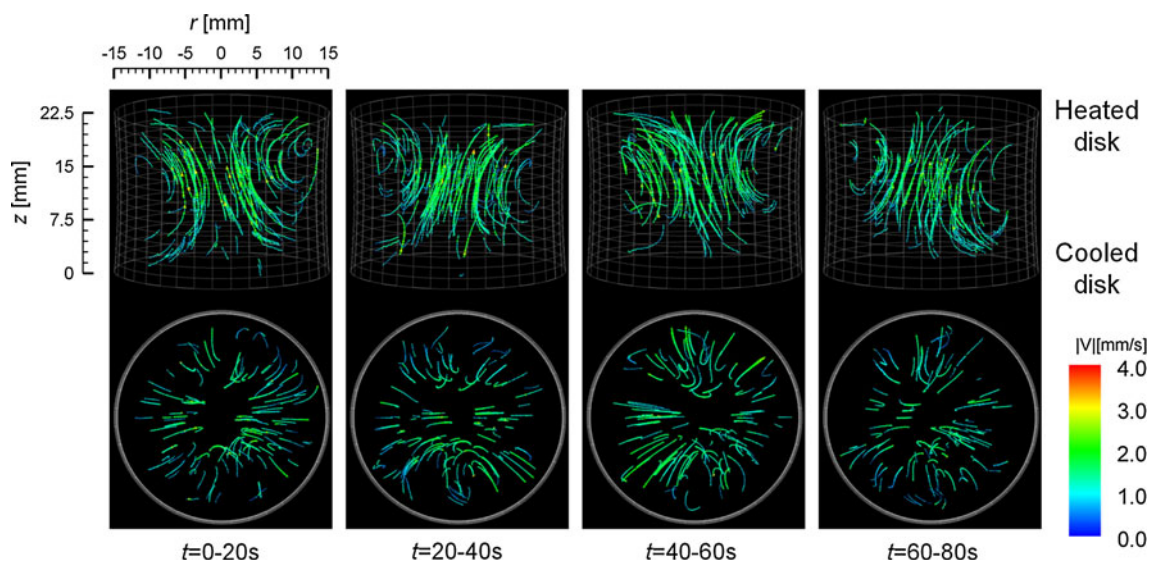


Fig. 6 Particle trajectories measured for $Ar = 0.75$ and $\Delta T = 7.9$ K

oscillation period is 40 s, and each plot presents the particle trajectories for 20 s. The particle trajectories exhibit a back-and-forth oscillation of a diagonally inclined flow pattern. The oscillation takes place in a fixed radial direction, and therefore, this oscillation is classified as a standing wave with $m = 1$, where m is an azimuthal mode number of oscillation. The flow pattern shows the presence of a single pair of vortices, one in the left side and the other in the right side of the liquid bridge. No multi-roll structures are seen in this low Ar liquid bridge. The oscillatory flow pattern shown here is similar to those observed in the previous ground experiments (e.g., Fig. 3 in Schwabe 1981).

3.2.2 $Ar = 1.5$

Figure 7 shows the particle trajectories measured for $Ar = 1.5$, where Fig. 7a, b shows the results for

$\Delta T = 3.1$ K ($Ma = 2.44 \times 10^4$, $Ma/Ma_c = 1.03$) and $\Delta T = 11.2$ K ($Ma = 9.49 \times 10^4$, $Ma/Ma_c = 4.02$), respectively. The particle trajectories are viewed from two orthogonal directions so that their 3-D structures are recognized unambiguously. The durations of the particle trajectories are 80 and 15 s in Fig. 7a, b, respectively. These durations correspond to a half of the respective oscillation periods, T . Figure 7a(1), a(2) presents an orthogonal view of the oscillatory flow field at ΔT that is only slightly higher than ΔT_c . It is recognized that the particle trajectories in Fig. 7a(1) are slightly inclined to the diagonal direction while those in Fig. 7a(2) are vertically straight in the liquid bridge except for the region close to the heated disk where the particle trajectories start to spread radially. The oscillation of the flow field is recognized by the oscillation of the streaks marked with photochromic dye, as shown in Fig. 8. These streaks visualize the behavior of the

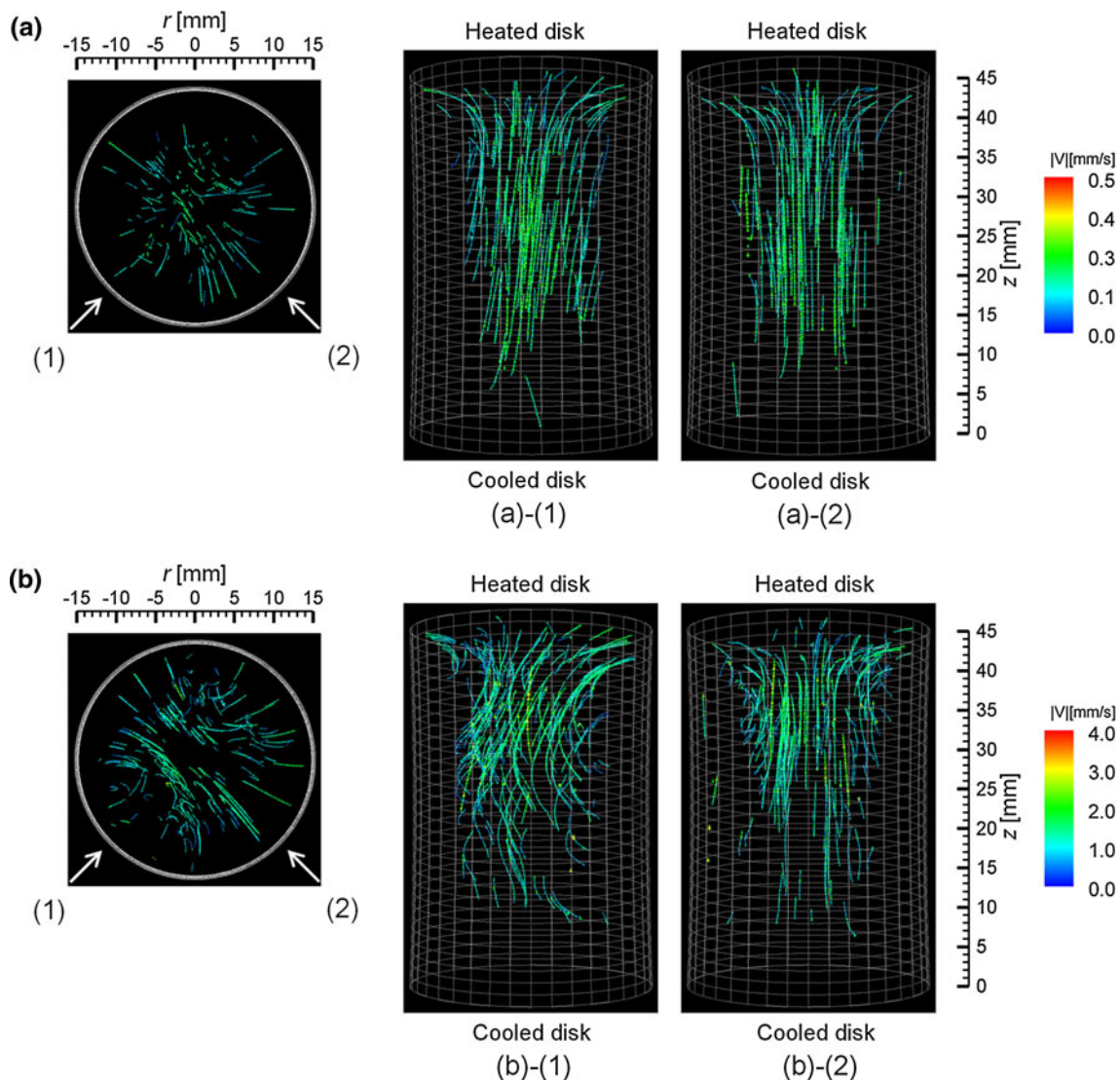


Fig. 7 Particle trajectories measured for $Ar = 1.5$ (a) just after the transition to oscillatory state and (b) at high Ma

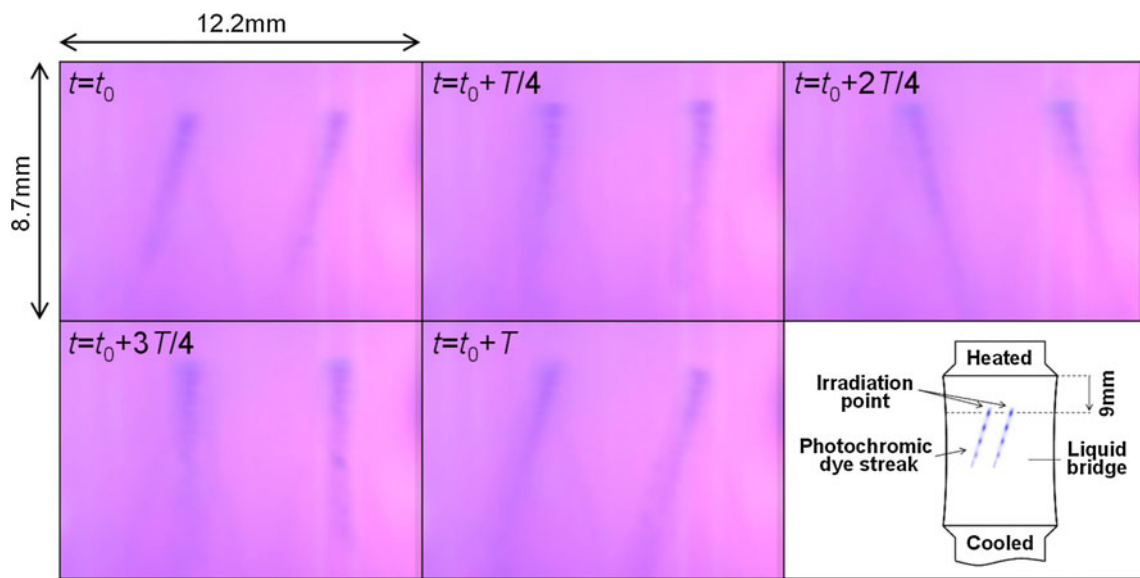
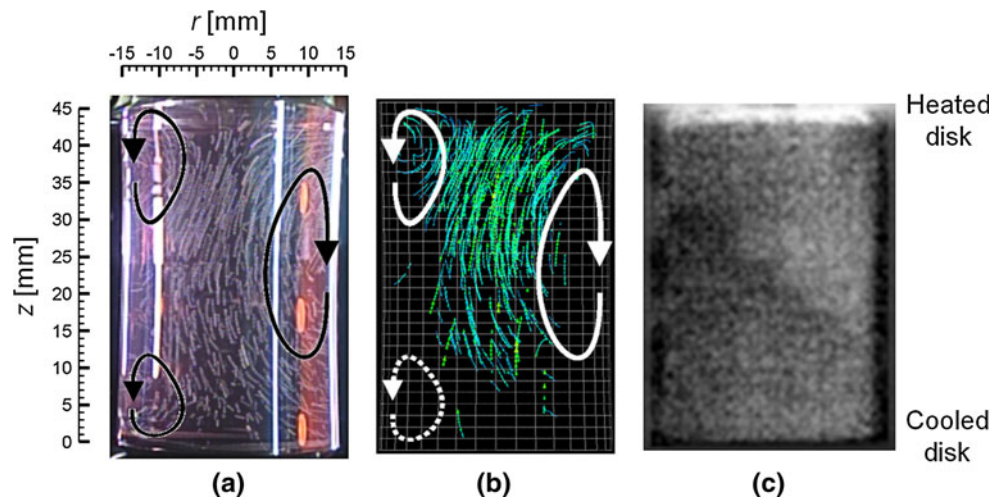


Fig. 8 Visualization of surface velocity by means of the photochromic dye activation method

Fig. 9 Flow structure for $Ar = 1.5$ and $\Delta T = 11.2$ K acquired by (a) the side-view camera, (b) 3-D PTV, and (c) the IR camera



surface flow at two irradiations points located 9 mm from the heated disk. The streaks about 5 mm long in the figure show an oscillatory behavior with a period of 30 s; they are inclined to the left at $t = t_0$ and then to the right at $t = t_0 + 2T/4$, and they return to the initial position at $t = t_0 + T$. These results indicate that the entire flow field in this long liquid bridge is oscillating within a fixed meridional plane and therefore that this oscillation is in a standing-wave mode with $m = 1$. Figure 7b shows the oscillatory flow field at ΔT which is much higher than ΔT_c . The oscillatory flow pattern is still in the standing-wave mode with $m = 1$. An interesting feature is that the particle trajectories seen in Fig. 7b(1) carry a lot of small vortical structures (VSs hereafter).

To understand the flow mechanisms responsible for the VSs mentioned above, further data analysis was carried out. Figure 9 shows (a) the 2-D particle trajectories for 4 s

seen by the side-view camera (cf. Fig. 3), (b) the 2-D projection of 3-D particle trajectories for 4 s measured with 3-D PTV, and (c) the gray-level image of surface temperature fluctuation visualized with the IR camera. All these figures present the results at the same oscillation phase. Note that the phase superposition over a total of six oscillation cycles is again applied to the particle trajectories shown here. Also note that the particle trajectories shown in Fig. 9b are those projected to the direction of the side-view camera so that the particle trajectories in Fig. 9a, b can be compared. Figure 9a shows the presence of three VSs at the locations marked by the arrows. Two VSs, both in counterclockwise rotation, exist near the surface (the left surface in the figure), and they are reminiscent of the multi-roll structures reported by Schwabe (2005) in his long liquid bridge ($Ar = 2.5$). A single VS exists near the other surface (the right surface in the figure), resulting in a

nonaxisymmetric flow pattern in the liquid bridge. Such flow patterns seen in Fig. 9a are also recognized in Fig. 9b except for the region near the cooled disk where only few 3-D particle trajectories are obtained. As shown later, these VSs are found to travel from the heated disk to the cooled disk. The nonaxisymmetric feature is also seen in the surface temperature fluctuation shown in Fig. 9c. There is an inclined interface between high and low temperature regions (white and black regions in the figure), and it is shown later that the interface travels in the same direction and with the same speed as the VSs.

Figure 10a shows the distributions of the gray level within the axial bands marked in the original IR image (Fig. 10b) and in the corresponding temperature fluctuation image (Fig. 10c). Note that Fig. 10c is identical to Fig. 9c. The gray level extracted from the original IR image increases gradually from the cooled disk toward the heated disk except for the region near the disks where the gray level changes significantly. Such distribution is consistent

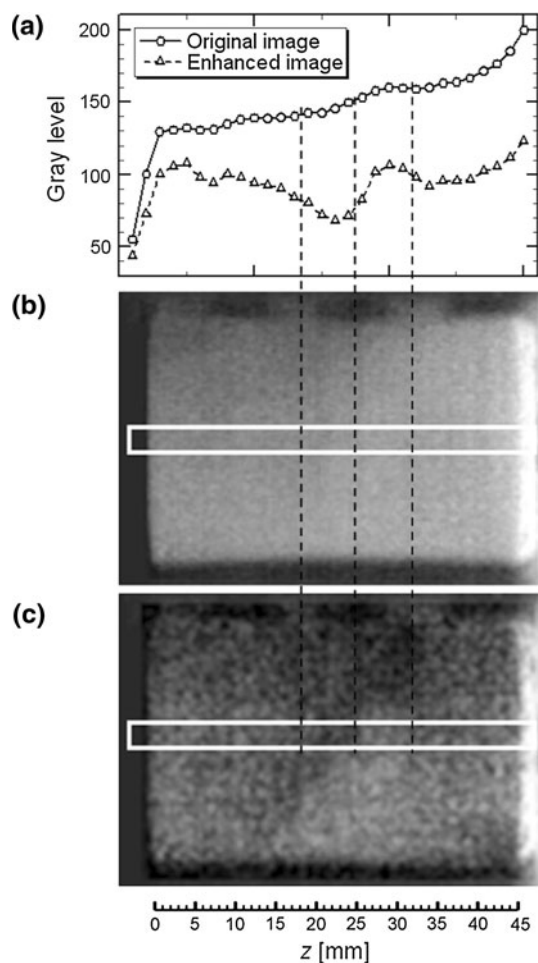


Fig. 10 Profiles of the gray level in (a) the original IR image and (b) the subtracted IR image corresponding to the surface temperature fluctuations

with the surface temperature profile reported previously (e.g., Figs. 5, 6 in Kamotani et al. 1984). The temperature gradient, which is evaluated from the gray-level gradient for $z = 5\text{--}40$ mm, is 0.023 K/mm. It corresponds to $0.092\Delta T/H$, which is very close to the value of $0.1\Delta T/H$ assumed by Schwabe (2005) in the comparison between his experimental result and the linear stability analysis of Xu and Davis (1984). The gray-scale variation, which is corresponding to the surface temperature fluctuation, is more recognizable in Fig. 10c, where the mean gray-scale image is subtracted from the instantaneous gray-scale image. It is found that the inclined interface between hot and cold regions is corresponding to the narrow area where the surface temperature decreases and then increases steeply. Comparison between Fig. 9a, c indicates that this narrow area of steep temperature variations is associated with the two VSs marked in Fig. 9a, one in the left side near the heated disk and the other in the right side.

The temporal behaviors of flow and temperature fields are examined. Figure 11 presents the projected particle trajectories plotted at a time interval of $1/6$ oscillation period. Note that the phase superposition over six oscillation periods is applied to these plots. Figure 11a, which is identical to Fig. 9b, exhibits two VSs near the left surface and one VS near the right surface. The VS near the left surface and near the heated disk grows with time (Fig. 11a–c) and occupies the left half of the liquid bridge at $t = t_0 + 3T/6$. At this phase of oscillation, two VSs are seen near the right surface. One of them near the heated disk starts to grow with time until it occupies the right half of the liquid bridge at $t = t_0$. The feature that the flow patterns in Fig. 11a–c and those in Fig. 11d–f are symmetrical is consistent with the fact that the oscillation is in a standing-wave mode with $m = 1$.

Figure 12 presents a time-series plots of the gray-scale images of surface temperature fluctuation. The VSs seen in Fig. 11 are superposed here for better understanding of the relation between surface temperature fluctuations and flow structures. Note that Fig. 12a is identical to Fig. 9c. It is observed that the inclined temperature interface between hot and cold region travel from the heated disk toward the cooled disk. This propagation direction is the same as that for VSs. The inclination angle of the temperature interface seen in Fig. 12a–c is opposite to that seen in Fig. 12d–f. The temperature interface and the VSs travel with the same speed, thus keeping their mutual configuration (in other words, their phase relationship) the same. This feature strongly suggests that the oscillation of flow and temperature fields is due to the HTW instability as shown by Xu and Davis (1984) in their linear stability analysis.

The characteristics of the HTW observed presently are discussed in comparison with those reported by Xu and Davis (1984) and Schwabe (2005), where the former is

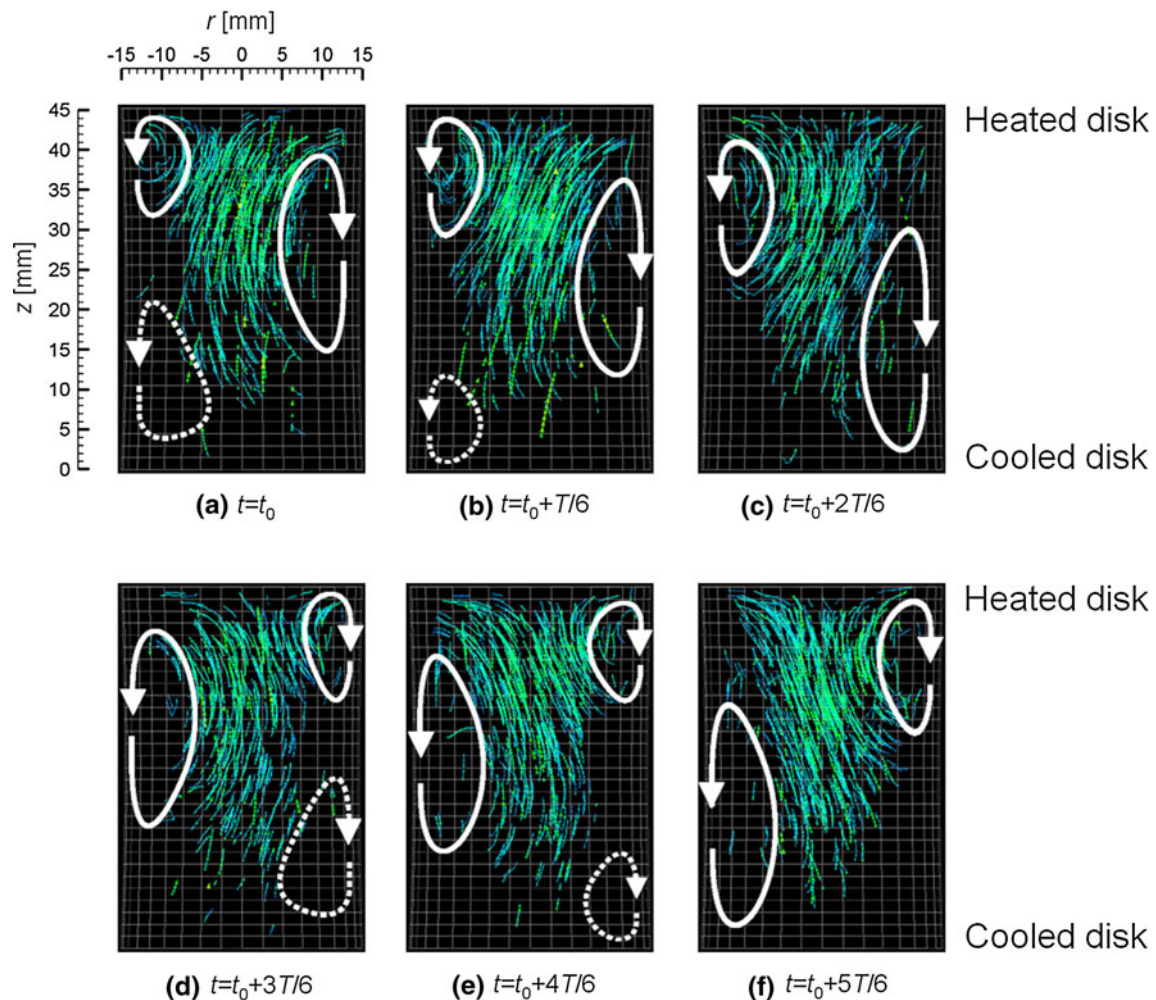


Fig. 11 Time evolution of particle trajectories measured by using 3-D PTV

abbreviated as XD and the latter as SW in this section. Note that the characteristics are evaluated at $Ma \sim 2Ma_c$ in SW and at $Ma \sim 4Ma_c$ presently. Table 1 summarizes the main characteristics of HTW together with the conditions of the liquid bridge. The mode of oscillation observed in the present experiment is a standing wave with $m = 1$ while it is a spirally traveling wave with $m = 1$ in SW and XD. In the linear stability analysis, two spirally traveling waves with opposite rotational directions can exist simultaneously and their superposition will result in a standing wave. The mode of oscillation in SW is reported as a spirally traveling wave. But the fact that their azimuthal phase speed deduced from thermocouple signals vary depending on the azimuthal position does not exclude the possibility of a standing-wave mode in his experiment.

The HTW in the present experiment propagates in the direction from the heated disk toward the cooled disk as shown in Fig. 12. This propagation direction is the same as

that reported by XD but opposite to that measured by SW, who reported the propagation of HTW from the cooled disk toward the heated disk and ascribed this difference to the effect of large heat loss in his experiment. The inclination angle of the wavefront of the present HTW is 37° , where it is defined as an angle between the direction normal to the wavefront and the direction of the liquid-bridge axis. This value may be compared with the angle between the propagation direction and the axial direction for spirally traveling waves. The values are 47° and 44° in SW and XD, respectively. The present inclination angle is close to the propagation angles in SW and XD. But, it is important to note that the observed features of standing-wave oscillations are dependent on the azimuthal position from which the observation is made. This means that the inclination angle might appear differently if the observation is made from different azimuthal positions. This must be taken into account in the comparison.

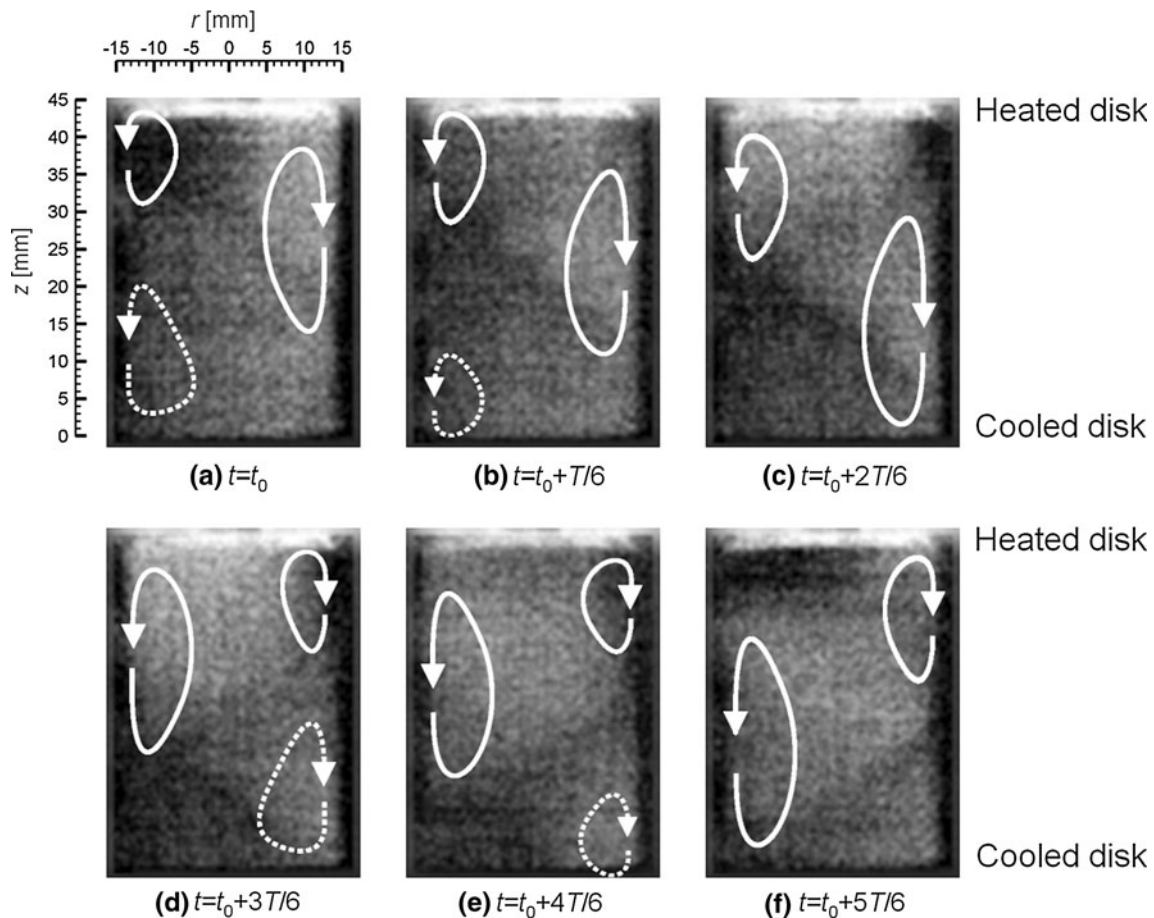


Fig. 12 Time evolution of surface temperature fluctuations viewed by IR camera

Table 1 Main characteristics of the hydrothermal wave and the conditions of the liquid bridge

	Present	Schwabe (2005)	Xu and Davis (1984)
Fluid	5cSt silicone oil	2cSt silicone oil	–
Pr	67.0	28.0	67.0
D	30 mm	6 mm	–
Ar	1.5	2.5	∞
Mode of oscillation	Standing	Spirally traveling	Spirally traveling
Azimuthal mode number	$m = 1$	$m = 1$	$m = 1$
Propagation direction	Toward cooled disk	Toward heated disk	Toward cooled disk
Inclination angle	37°	47°	44°
Dimensionless oscillation frequency, \tilde{f}	3.0	2.1	∞
Dimensionless axial wavelength, $\tilde{\lambda}_z$	1.5	2.7	3.1

Dimensionless values of the oscillation frequency, \tilde{f} , and of the axial wavelength, $\tilde{\lambda}_z$, are also included in Table 1, where $\tilde{f} = f \cdot H^2 / (\alpha \sqrt{Ma})$ and $\tilde{\lambda}_z = \lambda_z / D$. This dimensionless oscillation frequency was proposed by Preisser et al. (1983), and it becomes infinite for an infinitely long liquid bridge as assumed in XD. The value of \tilde{f} is 3.0

in the present, while it is 2.1 in SW. Although their strict comparison is difficult because of the difference in Ma and Ar , these experimental values are considered to be comparable to each other. The values of $\tilde{\lambda}_z$ are 1.5, 2.7, and 3.1 in the present, SW and XD, respectively. SW interpreted his value to be in good agreement with the value of XD.

But, it is interesting to point out that the values of 1.5 in the present and 2.7 in SW are very close to the respective values of Ar (i.e., 1.5 and 2.5). Not shown here, it is also found that $\tilde{\lambda}_z \sim 2.0$ for $Ar = 2.0$ in the present space experiment. These experimental results strongly suggest that the axial wavelength of HTW observed in a long liquid bridge is approximately the same as the length of the liquid bridge. This may predict that the maximum value of the axial wavelength is π for the liquid bridge of the Rayleigh limit (i.e., $Ar = \pi$). The value of 3.1 in XD for an infinitely long liquid bridge is close to this maximum value, but it is not the case for Pr other than 67.0 because $\tilde{\lambda}_z$ given by XD is appreciably dependent on Pr .

4 Conclusions

This paper reports the results of 3-D PTV measurement of the Marangoni convection in liquid bridges of high Prandtl number fluid. The microgravity environment on the International Space Station is exploited to generate large liquid bridges, 30 mm in diameter and up to 60 mm in length. The working fluid is 5cSt silicone oil. 3-D PTV is used to reveal complex flow patterns that appear after the transition of the flow field to oscillatory states. An IR camera is also used to visualize the surface temperature and its fluctuation of the liquid bridge. The present 3-D PTV measurement is verified through the comparison between the measured and the computed axial velocity profiles in a steady convection.

It is found that a standing-wave oscillation having an azimuthal mode number equal to one appears in the long liquid bridges. The flow pattern for $H = 22.5$ mm ($Ar = 0.75$) shows a single pair of oscillatory vortical structures that are similar to those observed in the previous ground experiments. For the liquid bridge 45 mm in length, the standing oscillation of the flow field is observed in a meridional plane of the liquid bridge and the flow field exhibits the presence of multiple vortical structures traveling from the heated disk toward the cooled disk. The oscillation of the flow field is related to the nonaxisymmetric presence of those vortical structures. It is also found that such flow behaviors are associated with the propagation of surface temperature fluctuations. These results indicate that the oscillation of the flow and temperature field is due to the propagation of the hydrothermal waves. Their characteristics are discussed in comparison with some previous results for long liquid bridges. It is shown that the axial wavelength of the hydrothermal wave observed presently is comparable to the length of the liquid bridge and that this result disagrees with the previous linear stability analysis for an infinitely long liquid bridge.

Acknowledgments The author would like to thank JAXA and the members of the present space experiments for their assistance to perform this study. The authors also acknowledge that a part of this study was supported by Grant-in Aid for Scientific Research (B#21360101) from the Japan Society for Promotion of Science (JSPS).

References

- Chernatinsky VI, Birikh RV, Briskman VA, Schwabe D (2002) Thermocapillary flows in long liquid bridges under microgravity. *Adv Space Res* 29(4):619–624
- Kamotani Y, Ostrach S, Vargas M (1984) Oscillatory thermocapillary convection in a simulated floating-zone configuration. *J Crystal Growth* 66:83–90
- Kawamura H, Ueno I (2006) Review on thermocapillary convection in a half-zone liquid bridge with high Pr fluid: onset of oscillatory convection, transition of flow regimes, and particle accumulation structure. In: Savino R (ed) *Surface tension-driven flows and applications*, Research Signpost, pp 1–24
- Kawamura H, Nishino K, Matsumoto S, Ueno I (2010) Space experiment of Marangoni convection on international space station. In *Proceedings of the 14th international heat transfer conference*, 8–13 August, 2010, Washington, USA (also submitted to the *Transactions of ASME, Journal of Heat Transfer*)
- Kuhlmann HC (1999) *Thermocapillary convection in models of crystal growth*. Springer tracts in modern physics, vol. 152. Springer, Berlin, Heidelberg
- Mass HG, Gruen A, Papanioniou D (1993) Particle tracking velocimetry in three-dimensional flows. *Exp Fluids* 15:133–146
- Nishimura M, Ueno I, Nishino K, Kawamura H (2005) 3D PTV measurement of oscillatory thermocapillary convection in half-zone liquid bridge. *Exp Fluids* 38(3):285–290
- Nishino K, Kasagi N, Hirata M (1989) Three-dimensional particle tracking velocimetry based on automated digital image processing. *J Fluids Eng-T ASME* 111:384–391
- Nishino K, Yamawaki M, Takami M (1995) Three-dimensional flow visualization and measurement of suspended liquid bridge. *J Jpn Soc Microgravity Appl* 12(4):205–213
- Nishino K, Kawamura H, Emori T, Iijima Y, Kawasaki K, Makino K, Yoda S, Kawasaki H (1998) Simultaneous observation of three-dimensional flow and surface temperature of unsteady Marangoni convection in a liquid bridge (in Japanese). *J Jpn Soc Microgravity Appl* 15(3):158–164
- Ostrach S (1983) Fluid mechanics in crystal growth—The 1982 freeman scholar lecture. *Transactions of the ASME. J Fluids Eng* 105:5–20
- Preisser F, Schwabe D, Scharmann A (1983) Steady and oscillatory thermocapillary convection in liquid columns with free cylindrical surface. *J Fluid Mech* 126:545–567
- Schwabe D (1981) Marangoni effects in crystal growth melts. *Physico Chemical Hydrodynamics* 2(4):263–280
- Schwabe D (2005) Hydro thermal waves in a liquid bridge with aspect ratio near the Rayleigh limit under microgravity. *Phys Fluids* 17:112104
- Shevtsova V, Mialdun A, Kawamura H, Ueno I, Nishino K, Lappa M (2011) Onset of hydrothermal instability in liquid bridge. *Experimental benchmark*. *FDMP* 7(1):1–28
- Tiwari S, Nishino K (2007) Numerical study to investigate the effect of partition block and ambient air temperature on interfacial heat transfer in liquid bridges of high Prandtl number fluid. *J Crystal Growth* 300:486–496
- Xu JJ, Davis SH (1984) Convective thermocapillary instabilities in liquid bridges. *Phys Fluid* 27(5):1102–1107

Yano T, Nishino K, Kawamura H, Ohnishi M, Ueno I, Matsumoto S, Yoda S, Tanaka T (2010a) 3-D PTV measurement of Marangoni convection in liquid bridge in space experiment. In Proceedings of the 14th international symposium on flow visualization, 21–24 June, Daegu, Korea

Yano T, Nishino K, Kawamura H, Ueno I, Matsumoto S, Ohnishi M, Yoda S (2010b) 3-D flow measurement of oscillatory thermocapillary convection in liquid bridge in MEIS. Submitted to the J Japan Soc Microgravity Appl